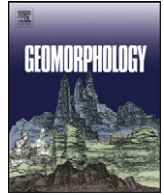


## ***Debris flow initiation in proglacial gullies on Mount Rainier, Washington***

The Faculty of Oregon State University has made this article openly available.  
Please share how this access benefits you. Your story matters.

<b>Citation</b>	Legg, N. T., Meigs, A. J., Grant, G. E., & Kennard, P. (2014). Debris flow initiation in proglacial gullies on Mount Rainier, Washington. <i>Geomorphology</i> , 226, 249-260. doi:10.1016/j.geomorph.2014.08.003
<b>DOI</b>	10.1016/j.geomorph.2014.08.003
<b>Publisher</b>	Elsevier
<b>Version</b>	Version of Record
<b>Terms of Use</b>	<a href="http://cdss.library.oregonstate.edu/sa-termsfuse">http://cdss.library.oregonstate.edu/sa-termsfuse</a>



# Debris flow initiation in proglacial gullies on Mount Rainier, Washington



Nicholas T. Legg <sup>a,\*</sup>, Andrew J. Meigs <sup>a</sup>, Gordon E. Grant <sup>a,b</sup>, Paul Kennard <sup>c</sup>

<sup>a</sup> Oregon State University, College of Earth, Ocean, and Atmospheric Sciences, Corvallis, OR 97331, USA

<sup>b</sup> United States Department of Agriculture, Forest Service, Pacific Northwest Research Station, 3200 Jefferson Way, Corvallis, OR 97331, USA

<sup>c</sup> Mount Rainier National Park, 55210 238th Ave E, Ashford, WA 98304, USA

## ARTICLE INFO

### Article history:

Received 30 September 2013

Received in revised form 17 July 2014

Accepted 3 August 2014

Available online 10 August 2014

### Keywords:

Debris flow

In-gully debris flow initiation

Glacier retreat

Climate change

Hazards

Cascade volcanoes

## ABSTRACT

Effects of climate change, retreating glaciers, and changing storm patterns on debris flow hazards concern managers in the Cascade Range (USA) and mountainous areas worldwide. During an intense rainstorm in November 2006, seven debris flows initiated from proglacial gullies of separate basins on the flanks of Mount Rainier. Gully heads at glacier termini and widespread failure of gully walls imply that overland flow was transformed into debris flow along gullies. We characterized gully change and morphology, and assessed spatial distributions of debris flows to infer the processes and conditions for debris flow initiation. Slopes at gully heads were greater than  $\sim 0.35 \text{ m m}^{-1}$  ( $19^\circ$ ) and exhibited a significant negative relationship with drainage area. A break in slope–drainage area trends among debris flow gullies also occurs at  $\sim 0.35 \text{ m m}^{-1}$ , representing a possible transition to fluvial sediment transport and erosion. An interpreted hybrid model of debris flow initiation involves bed failure near gully heads followed by sediment recruitment from gully walls along gully lengths. Estimates of sediment volume loss from gully walls demonstrate the importance of sediment inputs along gullies for increasing debris flow volumes. Basin comparisons revealed significantly steeper drainage networks and higher elevations in debris flow-producing than non-debris flow-producing proglacial areas. The high slopes and elevations of debris flow-producing proglacial areas reflect positive slope–elevation trends for the Mount Rainier volcano. Glacier extent therefore controls the slope distribution in proglacial areas, and thus potential for debris flow generation. As a result, debris flow activity may increase as glacier termini retreat onto slopes inclined at angles above debris flow initiation thresholds.

© 2014 Elsevier B.V. All rights reserved.

## 1. Introduction

Steep slopes and incompetent bedrock combine to make stratovolcanoes in the Cascade Range some of the most erodible bedrock landforms on Earth (Mills, 1976). In the Cascade Range in the northwestern United States, andesitic volcanoes stand well above the current and Quaternary-average equilibrium line altitudes of glaciers; glacial erosion at these elevations produces enormous sediment loads (Porter, 1989; Czuba et al., 2011, 2012). This sediment poses challenges to dam operators, river managers, and communities downstream by filling reservoirs, aggrading channels, and exacerbating flood risk (Czuba et al., 2010). Sediment transport and mass movement processes on volcanic slopes are therefore linked with management of downstream rivers. In addition to their role in sediment routing, debris flows threaten infrastructure immediately downstream. Moreover, recent debris flow episodes have raised concerns that increasing storm intensity, retreating glaciers, and

reduced snow-packs under a warming climate may cause more debris flows in the future.

Interrelationships between glaciers, runoff, and debris flow generation remain poorly understood. Limited understanding of conditions necessary for debris flow initiation in this environment prevents assessing effects of climate change and related factors on debris flow occurrence. Recent observations on Mount Rainier (Washington, USA) suggest that debris flow initiation has occurred in gullies passing through areas dominated by loose glacial till. These gullies show evidence of wall collapse and lateral expansion along their lengths, which may represent a source of sediment for the debris flows (Copeland, 2009; Lancaster et al., 2012). Gullies also begin at or very near to glacier termini and have no apparent slope failures that could have contributed debris flows from upstream glacier surfaces. Thus, debris flow initiation apparently occurs within gullies in the presence of, and perhaps in response to, surface runoff. Bed failure and/or progressive addition of sediment to surface runoff are possible mechanisms for debris flow initiation within gullies (Gabet and Bookter, 2008; Prancevic et al., 2014). The latter process is commonly referred to as sediment bulking (Wells, 1987). Debris flow initiation in gullies contrasts with more commonly discussed initiation style where shallow landslides on hillslopes liquefy

\* Corresponding author at: State of Washington, Department of Ecology, PO Box 47600, Olympia, WA 98504, USA. Tel.: +1 763 350 3052.

E-mail address: [ntlegg@gmail.com](mailto:ntlegg@gmail.com) (N.T. Legg).

and mobilize as debris flows in the absence of overland flow (Iverson et al., 1997). Debris flows beginning as landslides commonly initiate from hillslope hollows and run-out to and along channels downstream (Dietrich and Dunne, 1978).

Debris flow initiation induced by surface run-off is generally lesser understood than debris flow initiation from shallow landslides (Iverson, 1997; Coe et al., 2008; Kean et al., 2011; Prancevic et al., 2014). Prior studies of debris flows initiated in channels and gullies suggested bulking as the cause (Wells, 1987). Debris flows initiated in gullies are commonly observed in areas recently burned by wildfire (Cannon and Reneau, 2000; Gabet and Bookter, 2008; Santi et al., 2008). Monitoring of debris flow initiation by runoff has revealed that bed topography and resulting flow surges are important initiation variables (Kean et al., 2013). Recent theoretical formulations and supporting flume experiments find that channel bed failure at steep slopes is a primary debris flow initiation mechanism (Prancevic et al., 2014). Above channel slopes ranging from 15°–30°, critical Shields' stresses for fluvial sediment transport exceed those for debris flow transport, causing sediment transport by debris flows to become dominant (Lamb et al., 2008; Prancevic et al., 2014).

Studies of debris flows initiated in channels and gullies in environments recently burned by wildfire reveal possible analogs of sediment delivery to channels in glaciated environments (Wells, 1987; Meyer et al., 1995; Meyer and Wells, 1997; Cannon and Reneau, 2000; Gabet and Bookter, 2008; Santi et al., 2008). Reduced vegetation cover and ash deposition from burned vegetation reduce infiltration capacity, enhance runoff generation, and cause drainage networks to abruptly expand (Gabet and Bookter, 2008; Gabet and Sternberg, 2008). Material released during channel and gully expansion provides sediment that

has been connected with progressive transformation of overland flow to debris flow (Gabet and Bookter, 2008). Whereas glaciated catchments do not experience analogous changes in infiltration capacity, gullies often expand through recently deglaciated and unchanneled surfaces (O'Connor et al., 2001; Lancaster et al., 2012). It is therefore plausible that these young gullies actively expand during the largest storms in a manner similar to gullies in recently burned areas.

This study focuses on a set of seven debris flows that originated from proglacial areas of Mount Rainier during an intense storm in November 2006. Studying debris flows within a single meteorological event and roughly similar meteorological and hydrologic conditions across basins allows us to focus on the geomorphic conditions that influence debris flow initiation. The 2006 storm was unprecedented for the number of debris flows that initiated from separate basins; no prior historical events on Mount Rainier had so many debris flows (Fig. 1). Debris flows impacted infrastructure directly and indirectly by inducing channel avulsions. All told, debris flows and flooding inflicted \$36 million in infrastructure damage within Mount Rainier National Park boundaries (National Park Service, 2014).

This study seeks to characterize the landscape controls on debris flow initiation. Data are used to: (1) characterize the nature, setting, and change of debris flow gullies in detail, and (2) analyze basin-scale attributes that set local conditions for debris flow initiation. Aerial imagery and high-resolution topography derived from airborne laser swath mapping (ALSM) permit us to measure the morphology and change of debris flow gullies, and infer dynamics of debris flow initiation in areas inaccessible to field observation (James et al., 2007). Much of the analysis takes a comparative approach by analyzing differences in debris flow-producing basins (DFBs) and non-debris flow-producing

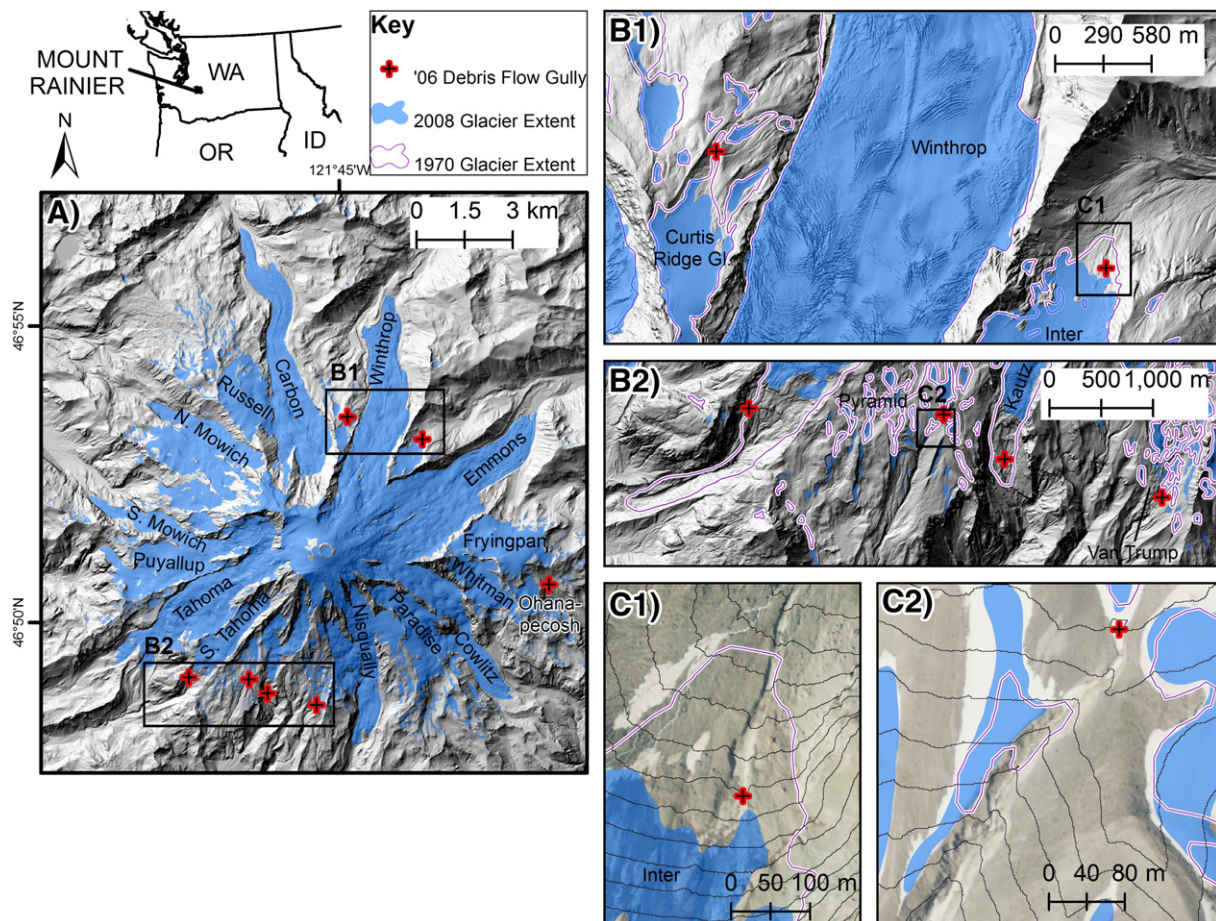


**Fig. 1.** Location map of Mount Rainier and debris flow gullies from the 2006 storm. (A) Hill-shaded topography of Mount Rainier. (B1 and B2) Hill-shaded topography produced from ALSM data. (C1 and C2) NAIP aerial images taken in 2009 with 10-m elevation contours.

basins (NDFBs) as defined by debris flow locations in the 2006 storm. This comparison is predicated on the assumption that spatial patterns reflect differences in debris flow potential between basins.

**2. Setting**

Mount Rainier is a stratovolcano of andesite-dacite composition and the highest peak (4392 m asl) in the Cascade Range. The volcano supports the greatest volume of glacier ice in the lower United States (Driedger and Kennard, 1984; Hildreth, 2007). Present-day glaciers generally extend greater distances from the summit on the north and northeast than on the south and west sides of the mountain; however, glacier size varies locally with the maximum basin elevation (Fig. 1). Mountain-wide glacier volume loss from 1970 to 2007/8 (corresponding glacier extents shown in Fig. 1) has been measured at approximately 14% (Sisson et al., 2011). With the exception of a brief glacial advance in the 1960s and 1970s, the loss represents a continuation of glacial ice retreat occurring since the culmination of the Little Ice Age around 1850 (Table 1; Sigafos and Hendricks, 1972; Burbank, 1981; Heliker et al., 1984). All of the gullies where debris flows were initiated in the 2006 storm dissect areas that were deglaciated after, and in many cases more recently than the end of the Little Ice Age (Fig. 1).

Both hydrologically-induced debris flows and volcanic lahars originate from Mount Rainier; this study focuses exclusively on the former, which can be distinguished from lahars by various criteria (Crandell, 1971; Scott et al., 1995; Vallance and Scott, 1997). Hydrologically-induced debris flows mobilize surficial debris with low clay-content and corresponding low cohesion. Lahars documented from Mount Rainier are cohesive, high clay-content debris flows that often result from partial collapse of the volcanic edifice. The largest recognized lahar – the Osceola Mudflow of ca. 5600 years BP – initiated from the north-eastern flank of Mount Rainier and inundated portions of the Puget Sound Lowland approximately 100 km downstream (Vallance and Scott, 1997). Whereas lahars have return intervals in the order of 500 years, hydrologically-induced debris flows had decadal return

intervals during the past century (Scott et al., 1995). Hydrologically-induced debris flows generally travel less than 10 km from the summit and begin during rain storms or from glacier outburst floods (Walder and Driedger, 1994a,b). This study focuses on debris flows that begin during rain storms. Whereas the source of water is different, mechanisms of debris flow initiation from glacial outburst floods are likely similar.

**3. 2006 storm**

On November 6 and 7, 2006, a narrow and very moist air mass, termed an “Atmospheric River”, hit Mount Rainier from the southwest and dropped approximately 45 cm of rain over a 42-hour period (Neiman et al., 2008). Atmospheric River storms bring warm and moist air from tropical latitudes, drop heavy rain at high elevations, and melt antecedent snow packs (if present) (Neiman et al., 2008). During the most intense period of the storm, the National Resource Conservation Service (NRCS) Paradise Snowpack Telemetry (SNOTEL) station (7.6 km SSE of Mount Rainier summit; 1560 m asl; 46.78°N, 121.75°W) recorded average rainfall rates of approximately 0.9 cm h<sup>-1</sup>, with a maximum of 2.0 cm h<sup>-1</sup> (Fig. 2). For the duration of the storm, the Paradise SNOTEL station recorded snow-water equivalent less than 1 cm, and temperatures above freezing (Fig. 2). During the same period at the Morse Lake SNOTEL station (22 km ENE of Mount Rainier summit; 1645 m asl; 46.91°N, 121.48°W), rainfall intensity averaged 0.4 cm h<sup>-1</sup> with a maximum observed intensity of 0.8 cm h<sup>-1</sup>, suggesting orographic enhancement of storm precipitation, although the distance of the Morse Lake SNOTEL station from the summit may exaggerate the apparent orographic effect across the Mount Rainier edifice alone. Both the south-draining United States Geological Survey (USGS) Nisqually River gauging station at National (USGS ID: 12085000) and north-draining Carbon River gauging station at Fairfax (USGS ID: 12094000) recorded greater than 100-year discharges and floods of record. Whereas precipitation data from the SNOTEL sites suggest an orographic effect; gauging data suggest that flooding was of similar magnitude with respect to

**Table 1**  
Characteristics of the proglacial areas (PGAs) studied.

Glacier name	PGA area (km <sup>2</sup> )	Total extracted network length (m)	Drainage density (m m <sup>-2</sup> )	PGA elevation (m asl)			PGA mean slope (m m <sup>-1</sup> )	PGA max drainage area (km <sup>2</sup> )	1970–2007/8 glacier retreat (m) <sup>a</sup>
				Min	Mean	Max			
<i>NDFB</i>									
Cowlitz	1.02	9393	0.0092	1491	1640	1905	0.40	15.564	475
Emmons	0.18	2867	0.0158	1469	1498	1579	0.26	8.803	–130
Flett	0.81	8166	0.0101	1954	2081	2255	0.45	0.659	115
Fryingpan (East)	0.44	4866	0.0110	1778	1943	2074	0.37	2.050	110
Fryingpan (West)	0.71	8789	0.0123	1773	1918	2156	0.38	2.737	110
Nisqually	0.59	3966	0.0068	1343	1547	1846	0.66	12.081	300
North Mowich	0.81	8901	0.0110	1480	1683	2209	0.63	8.613	230
Paradise	2.09	21,168	0.0101	1774	1979	2253	0.35	2.502	75
Puyallup	0.12	2669	0.0224	1599	1722	1868	0.65	2.634	90
Russell	2.21	19,364	0.0088	1744	2053	2400	0.38	1.546	120
South Mowich	0.24	2935	0.0122	1482	1653	1893	0.61	7.191	260
South Mowich (south terminus)	0.12	1762	0.0145	1378	1499	1729	0.64	2.357	260
Tahoma	0.35	3495	0.0101	1503	1634	1803	0.40	5.246	45
Tahoma (west terminus)	0.61	7717	0.0126	1485	1656	1841	0.47	9.793	45
Whitman	0.56	7178	0.0129	1972	2243	2454	0.56	3.305	60
Mean	0.72	7549	0.0120	1615	1783	2018	0.48	5.672	144
<i>DFB</i>									
Curtis Ridge <sup>b</sup>	0.43	4547	0.0105	2110	2354	2600	0.53	2.633	75
Inter	0.32	5441	0.0171	1964	2109	2322	0.49	1.218	210
Kautz	0.96	11,661	0.0121	1501	1951	2417	0.69	4.868	70
Ohanapecosh	1.26	17,342	0.0137	1687	2031	2531	0.56	3.584	140
Pyramid	0.84	9661	0.0115	1878	2205	2474	0.42	1.645	150
South Tahoma	0.77	8802	0.0115	1496	1832	2274	0.70	3.120	300
Van Trump	0.61	6761	0.0111	1820	2116	2450	0.48	1.731	135
Mean	0.74	9174	0.0125	1779	2085	2438	0.55	2.685	154
p-Value	0.935	0.477	0.682	0.137	0.003	0.000	0.179	0.0304	0.8361

<sup>a</sup> Data from Sisson et al. (2011); negative retreat values indicate advance.

<sup>b</sup> Unnamed glacier located on west-bounding ridge of the Winthrop Glacier.

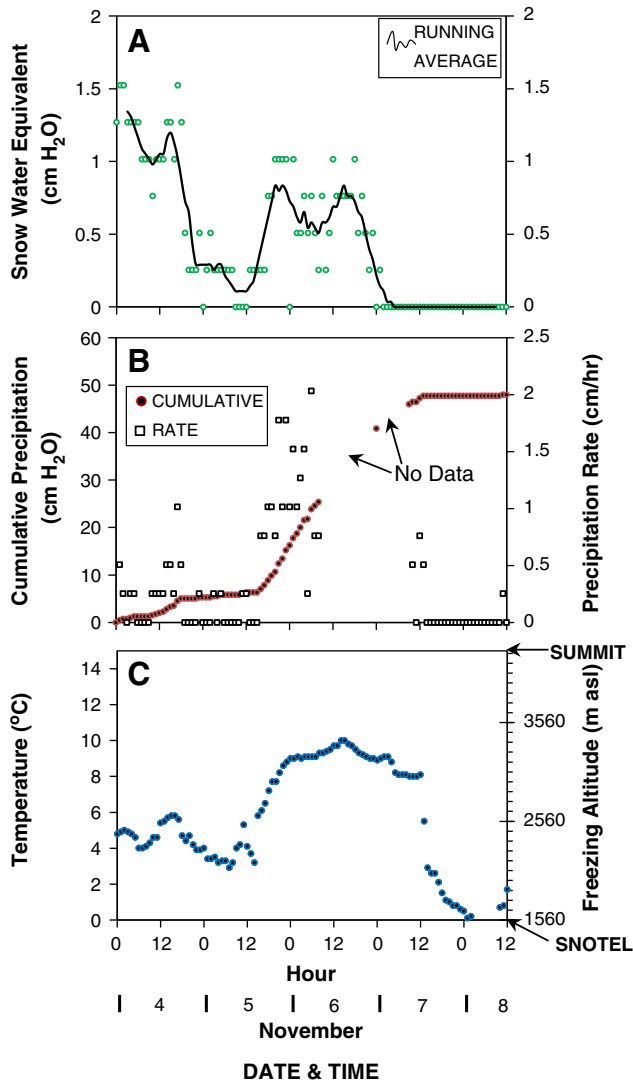


**Fig. 2.** Meteorological and snow data for the 2006 storm. Snow water equivalent (SWE, A), precipitation (B), and temperature (C) collected at the Paradise SNOTEL station (NRCS, 1560 m asl; 46.78°N, 121.75°W) in a period spanning the November 2006 storm are shown. Freezing altitudes (C) are estimated based on a temperature lapse rate of 5.5 °C per km altitude.

each basin's hydrographic record. Reconnaissance by National Park Service employees and Copeland (2009) following the storm recorded evidence of debris flows from six basins, including those containing the South Tahoma, Pyramid, Kautz, Van Trump, Inter, and Curtis Ridge glaciers (Fig. 1). As discussed later in this paper, a seventh debris flow initiated in 2006 from near the Ohanepcosh Glacier was identified in this work.

#### 4. Methods

In this study, we (1) characterized the nature and setting of gullies that initiated debris flows in a single storm in 2006, and (2) analyzed basin-scale attributes that control debris flow initiation near glaciers.

##### 4.1. General methods and data processing

Remotely sensed data from the National Aerial Imagery Program (NAIP, 1-m spatial resolution) including aerial photography and airborne laser swath mapping (ALSM) topographic data allowed us to measure gully change resulting from the 2006 storm and extract topographic

and hydrologic characteristics of the landscape. NAIP images taken in the summers of 2006 and 2009 bracketed the November 2006 storm. ALSM data were collected in September 2007, and September and October 2008, obtaining approximately 1.5–3.5 ground-classified points per m<sup>2</sup> in the sparsely vegetated areas focused on here.

Using standard flow accumulation algorithms, we extracted drainage networks from 4-m gridded digital elevation models (DEMs) down-sampled from ALSM data (Tarboton et al., 2006). A lower drainage area threshold of 10,000 m<sup>2</sup> used to extract drainage networks was based on approximate drainage areas measured at rill, gully and channel head locations in sparsely vegetated areas. We used our combined air-photo and ALSM time-series to visually scan basins for expanded gullies to identify debris flows not originally recorded in the 2006 storm (Copeland, 2009). Where undocumented expanded gullies were visible, we identified and mapped debris flow deposits in downstream areas dating to the same time period using established field criteria for identifying debris flows such as poorly sorted deposits with boulder concentrations at the surface, abraded tree boles, and landforms (Costa, 1988; Pierson, 2005).

##### 4.2. Initiation zone characterization

To characterize geometry changes and estimate volumes of sediment released from gully walls, plan-view changes were measured along one debris flow gully that initiated a debris flow in November 2006 in the Pyramid Glacier proglacial area (panel C2 in Fig. 1). Of the 2006 debris flow gullies, the Pyramid gully had the least snow coverage at the dates of the aerial image capture, which allowed us to measure horizontal width change in detail (Fig. 3). Whereas expansion was apparent in other basins (and documented by Copeland, 2009), snow coverage obscured gullies such that detailed measurements of gully change for the other gullies was impossible. The Pyramid gully is approximately 1.2-km long, with a longitudinal gradient of 24° near its head at the Pyramid glacier terminus. The gully runs along a Little Ice Age lateral moraine in an un-vegetated area covered by glacial till (Fig. 4), and enters a bedrock channel at an approximate gradient of 10° (Burbank, 1981).

To analyze planform changes in the Pyramid gully longitudinally, we digitized outlines of the debris flow gully in 2006 and 2008, subdivided each outline into 58, 20-m longitudinal segments (Fig. 3), and measured average width change ( $\Delta w$ ; segment area change in plan-view divided by segment length). Fig. 5 shows a simple model of gully geometry that allowed estimation of volume change from measurements of plan-view change and 2008 ALSM topography. This model of volume change required the assumption that gully wall slope ( $\alpha$ ) and bed elevations were unchanged by debris flow passage, and measurement of hillslope angle ( $\theta$ ) above the gully margin. Width change in the horizontal plane ( $\Delta w_h$ ) was calculated as:

$$\Delta w_h = \frac{(\Delta w * (\tan \alpha - \tan \theta) * \sin(90^\circ - \alpha))}{\sin \alpha} \quad (1)$$

where  $\alpha$  is the hillslope angle adjacent to gully margins. Cross-sectional area change ( $\Delta A$ ) for each segment was calculated as:

$$\Delta A = \Delta w * \sin \alpha * [(d / \sin \alpha) - (\Delta w * \tan \theta / 2d)], \quad (2)$$

where  $d$  is gully depth (Fig. 5). Area change multiplied by segment length (20 m) yielded segment volume change. These sediment volume estimates likely represent minimums considering that bed elevations likely changed. Finally, gully changes were correlated with longitudinal slope and hillslope contributing area. Contributing area from hillslopes revealed areas of topographic convergence of hillslopes (*sensu Hack and Goodlett, 1960*) and its control on gully wall failure.

We also characterized the seven debris flow gullies in terms of slope and drainage area to explore whether debris flow initiation occurred in

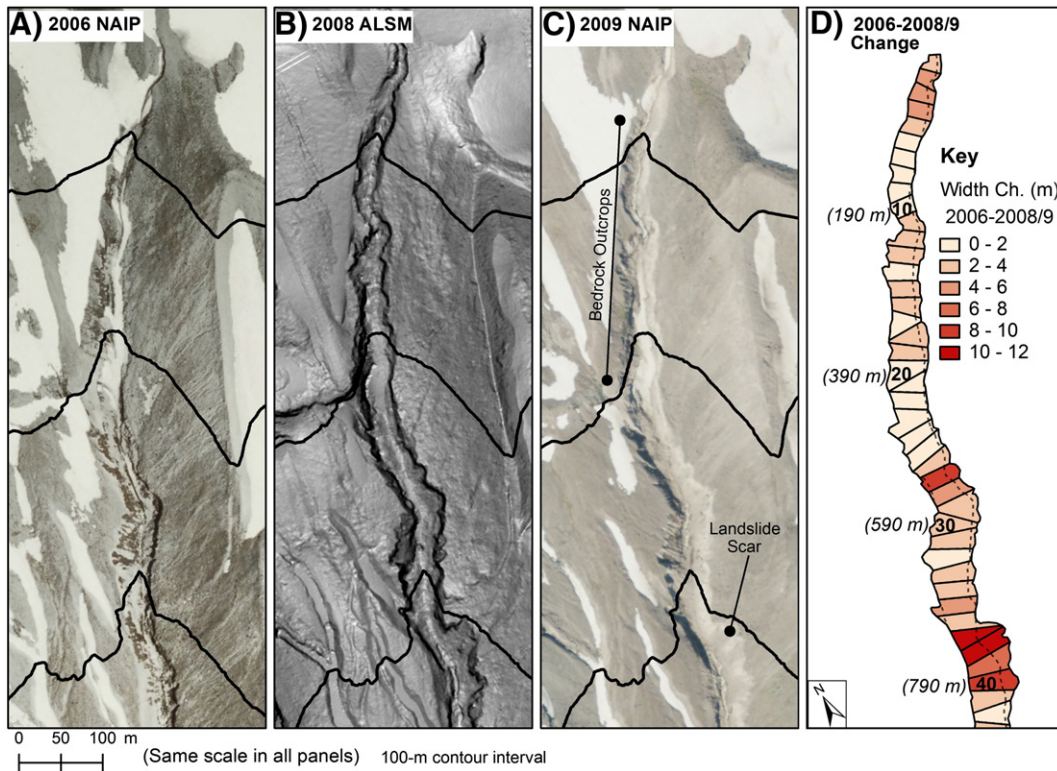


**Fig. 3.** Time-series of aerial imagery and the ALSM DEM for the Pyramid gully. (A) 2006, (B) 2008, (C) 2009, (D) temporal differences. The ALSM DEM in B has a grayscale color scheme with low slopes in light and steep slopes in dark. In D, 2006 (dashed) and 2008 gully (solid) outlines show gully expansion. Every tenth segment is labeled with distance downstream from the gully head and a segment number, which correspond to Fig. 9 segments. Segments are shaded by average width change.

unique process domains (Montgomery and Dietrich, 1994). In channels with steady flow, the product of slope and drainage area, which was assumed proportional to stream discharge (Hack, 1973), is a proxy for total stream power, or the rate of energy expenditure along a channel. Slope and drainage area therefore provide a measure of total energy available for sediment transport by fluvial processes within gullies, i.e., before sediment-laden flows transitioned to debris flows (Yang, 1972; Whipple and Tucker, 1999). Whereas assumptions of steady flow may be invalid in this environment, the exercise allowed examination of possible thresholds for debris flow initiation reflected among gullies. Because dangerous terrain prevented access to most gullies, slope and drainage area

measurements were taken along the gully with the greatest width change in each DFB. It was assumed that debris flow initiation occurred along the gully length defined by the upstream- and downstream-most points of visible width change in imagery. Slope and drainage area measurements were taken at upstream and downstream-most points, as well as at the midpoints of all links along a gully to characterize the range in slope and drainage area along gully lengths. The three sets of slope–area measurements are referred to as gully heads, downstream limits, and intermediate reaches (link midpoints).

We also measured infiltration capacity in un-vegetated proglacial areas in order to evaluate runoff generation on the upper slopes of the

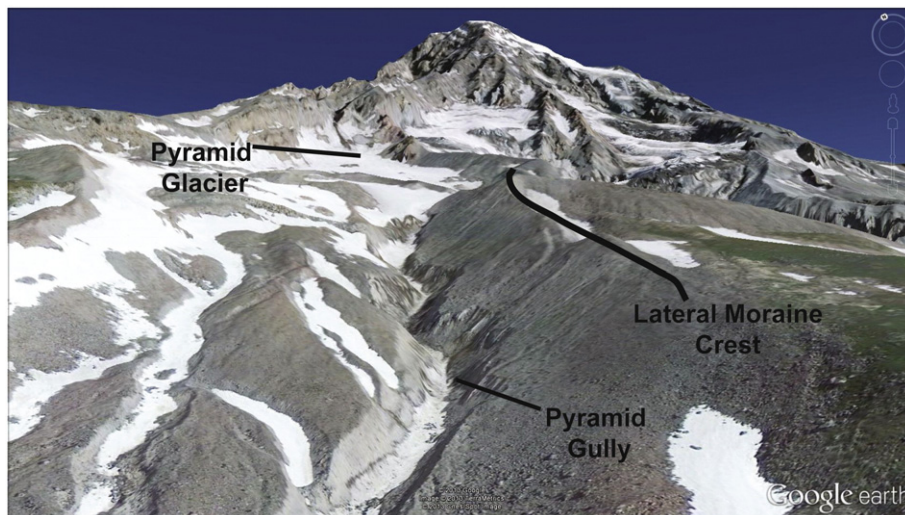


**Fig. 4.** Google Earth® oblique image of the Pyramid gully in 2012. The view is oriented to the northeast, looking upstream.

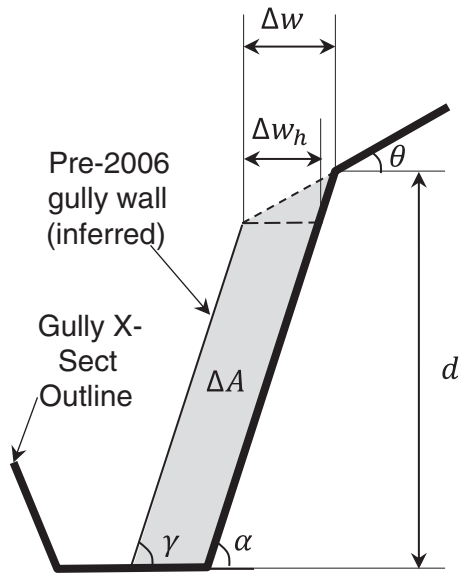


**Fig. 5.** Diagram of gully geometry used to convert width change ( $\Delta w$ ) measured from aerial imagery to volume change. Gully depth ( $d$ ), gully wall slope ( $\gamma$  before the storm,  $\alpha$  after the storm), and hillslope angle ( $\theta$ ) were all measured from 2008 ALSM data. Width change in the horizontal plane ( $\Delta w_h$ ) and area change in cross section ( $\Delta A$ ) were calculated.

mountain. Using a Mini Disk Infiltrometer (Decagon Devices®), infiltration capacity was measured at 19 un-vegetated, sediment-covered locations in four proglacial areas on Mount Rainier.

4.3. Drainage networks in proglacial areas

Analysis of drainage networks focused on proglacial areas because: (1) observations that recent debris flows on Mount Rainier have initiated in proglacial areas, and (2) abundant runoff and loose sediment in the front of glaciers implies that proglacial regions favor debris flow initiation. Proglacial areas were outlined as zones dominated by unconsolidated debris with sparse vegetation cover (<10% coverage) bounded on the up-valley end by the glacier terminus (Fig. 6; Sisson et al., 2011). Visible areas of bedrock exposure identified in aerial photography were omitted. Proglacial areas were mapped for all glaciers flanking Mount Rainier except the Carbon and Winthrop glaciers, because these two glaciers lack un-vegetated areas where slope exceeds  $10^\circ$ , the observed debris flow scour threshold by Benda and Cundy (1990). From drainage networks within mapped proglacial areas, longitudinal slope and drainage area were measured for each drainage network link in order to examine broader scale patterns of slope and drainage area relative to individual measurements of debris flow gullies (Fig. 6).

In order to examine slope–drainage area distributions in the two basin types (DFBs and NDFBs), a series of slope–drainage area partitions

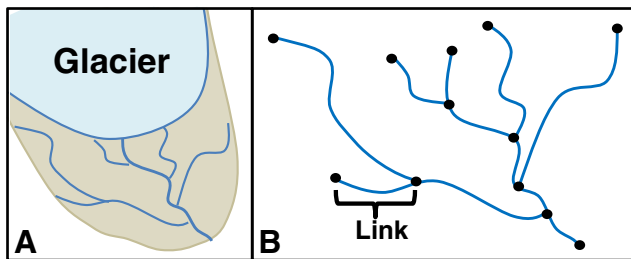


**Fig. 6.** Illustration of drainage network extraction from proglacial areas. (A) Hypothetical proglacial area with an algorithm-derived drainage network. (B) Drainage network divided into links at tributary junctions, each of which was used to extract slope and drainage area.

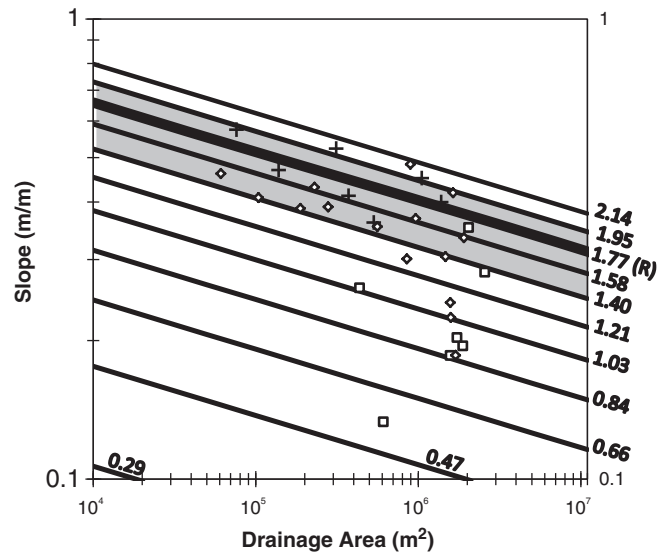


**Fig. 7.** Graph showing slope–drainage area partitions used in drainage network analysis. Crosses, diamonds, and squares refer to gully heads, intermediate reaches, and downstream limits of debris flow gullies ( $n = 7$ , see Fig. 10). Partition values are shown adjacent to individual lines and represent the value of the constant  $b$  in a power law equation of  $S = bA^c$ . Slope–drainage area ( $S$ – $A$ ) partitions are aligned parallel to the power regression equation ( $S = 1.769 A^{-0.107}$ ) for the gully heads of the seven debris flow gullies. Partition coefficients also correspond to horizontal axis values in Fig. 11. The gray shaded zone approximately encompasses the predominant  $S$ – $A$  trend in gully heads and intermediate reaches above  $\sim 0.35 \text{ m m}^{-1}$  (corresponding to gray box in Fig. 11).

were defined (Fig. 7). Slope–drainage area partitions were aligned parallel with a power-law regression of the slope and drainage area observed in debris flow gullies (Fig. 7). They allowed analysis of slope–drainage area distributions with respect to observed values in debris flow gullies. Metrics (defined below) were calculated using the number and length of links of the proglacial drainage networks exceeding each

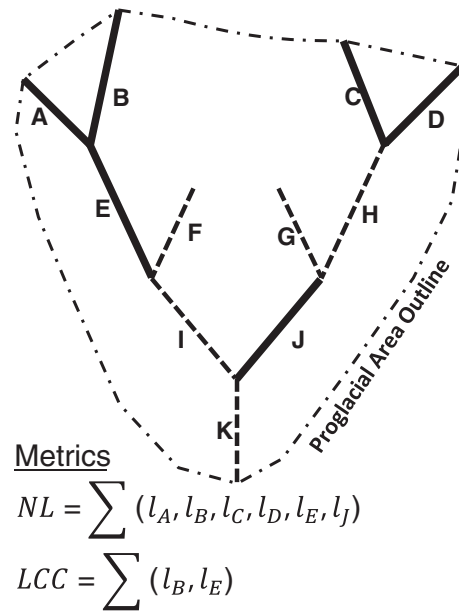


**Fig. 8.** Example calculations of metrics network length (NL) and longest connected channel (LCC) used to analyze slope and drainage area distributions in drainage networks (length,  $l$ ). Bold links (endpoints defined by tributary junctions) indicate those with slope and drainage area above a given partition. Dashed links are below the slope–drainage area partition.

partition (i.e., greater slope and drainage area), and were calculated for individual proglacial areas and averaged by basin type (DFB and NDFB). Differences in slope and drainage area distributions, as well as other general basin statistics were also evaluated using *t*-tests for differences of means assuming unequal variances.

Two metrics were used to analyze slope and drainage area distributions in proglacial areas: 1) the sum of drainage network length (NL) exceeding a slope–drainage area partition; and 2) the length of the longest connected channel (LCC) (Fig. 8). The NL metric captures distributions of slope and drainage area in proglacial drainage networks. Proglacial areas favorable for debris flow initiation were hypothesized to have a higher NL metric (a greater length of their drainage networks) along the slope–drainage area trend observed in gullies where debris flows were initiated. LCC incorporates observations that debris flow initiation occurs as a distributed process along a single gully or channel (Fig. 8). LCC was derived from a search for the length of the single longest set of connected links above a given slope–drainage area partition within each basin. Proglacial morphology, as reflected by NL, ought to correspond to areas of the drainage network with long channels, as reflected by LCC, of similar slope and drainage area. The longest channel or gully above some partition in slope–drainage area, however, serves as a measure of connectivity of the drainage network above a slope–drainage area partition and therefore may better differentiate debris flow potential in a given basin.

**5. Results**

*5.1. Initiation zone characterization*

Aerial imagery and field work confirmed the six known debris flows from the 2006 storm (Copeland, 2009) and a seventh previously unrecognized debris flow gully and downstream deposit. Aerial imagery revealed a gully that widened between 2006 and 2008 in the proglacial area of the Ohanapecosh Glacier (panel A in Fig. 1). In the field, poorly-sorted deposits, damaged tree boles, and boulder snouts and levees dating to the same time period suggested a debris flow had occurred in 2006 (Costa, 1988; Pierson, 2005).

The Pyramid debris flow gully widened on average 2.6 m horizontally between 2006 and 2008 along the 1.2-km reach (Figs. 3 and 9A). Due to this widening, we estimated that ~47,000 m<sup>3</sup> (± 6500 m<sup>3</sup> based on 1-m spatial resolution of remote sensing data) of sediment was evacuated from this single gully (Fig. 9B). Digitized outlines of the Pyramid gully in 2008 (ALSM) and 2009 (NAIP) were within the 1-m resolution of the two datasets. Gully expansion was distributed longitudinally as a series of wall collapses along the gully length, with horizontal width change ( $\Delta w_h$ ) exceeding zero in 51 of 57 (89%) 20-m gully segments. Minimal gully expansion occurred where bedrock exposures were visible, particularly on the northwest bank of the gully (Fig. 3).

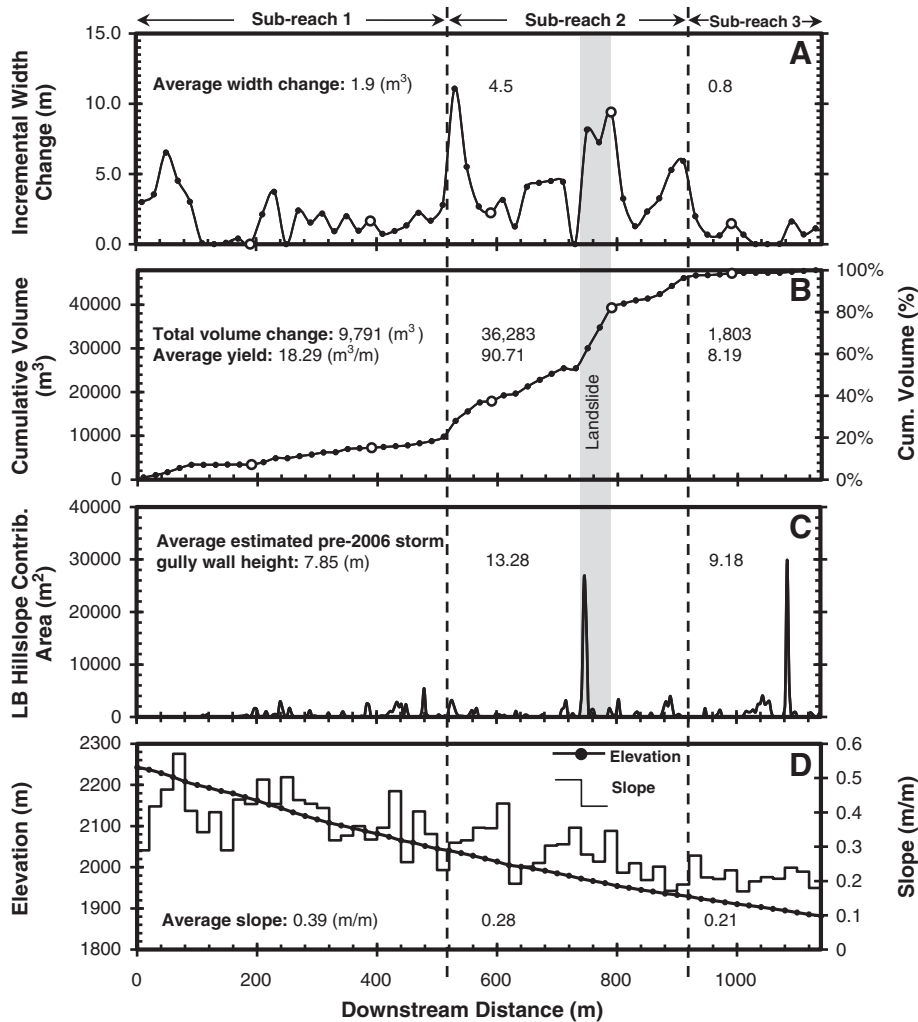


**Fig. 9.** Longitudinal data from the Pyramid debris flow gully. Data include incremental width change (A), cumulative volume change (B), hillslope contributing area from the east bank of the Pyramid gully (C, proxy for hillslope convergence), and slope and elevation with downstream distance in the Pyramid debris flow gully (D) estimated for each segment. Sub-reaches delineate distinct trends in volume change per unit gully length. Each panel contains representative values indicated for each sub-reach. Note the east bank contributing area (C) is extracted along a gully-parallel transect shifted approximately 20 m laterally from the gully bottom. Gully wall heights shown are estimates of pre-debris flow gully wall height figured trigonometrically (Fig. 5). Open circles in A and B show every tenth segments (Fig. 3D).

Gully segments with the greatest gully widening coincided with discrete bank failure scars and with locations along the gully where hillslopes had significant contributing area. Two un-channelized locations with contributing areas of  $>25,000 \text{ m}^2$  demonstrate how hillslope shape and implied water routing influence sediment input (Fig. 9C). The upstream-most location coincides with a visible bank failure scar encompassing a set of three consecutive 20-m segments, which account for  $\sim 28\%$  of the volume change in the Pyramid gully, whereas the second bank exhibited little change. Hillslope angles above the gully margin at these locations are  $27^\circ$  and  $16^\circ$ , respectively, suggesting that both the presence of water (due to convergent flow paths on hillslopes) and gradient on the hillslope influence failure of gully walls.

The volume change per unit gully length – commonly referred to as yield rate – is generalized by three sub-reaches of the gully (labeled sub-reaches 1, 2, and 3 moving downstream in Fig. 9), which may relate to processes of sediment recruitment occurring in the gully (Hungr et al., 1984). Sub-reaches were defined by breaks in the volume changed per unit length. Volume change per unit length is modest in sub-reach 1, high in sub-reach 2 ( $\sim 5$  times that of sub-reach 1), and negligible in sub-reach 3. The disparity in sediment yield between sub-reaches 1 and 2 corresponds with  $2.3\times$  and  $1.7\times$  increases in average width change and gully wall height from sub-reach 1 to 2, respectively (Fig. 9).

Measurements of individual gullies where debris flows were initiated in 2006 reveal varying patterns in slope–drainage area space (Fig. 10). Measurements at gully heads show the most apparent relationship between slope and drainage area, with a significant power law fit ( $n = 7$ ,  $R^2 = 0.477$ ). In general, the exponent ( $-0.107$ ) suggests that only minor reductions in gradient accompany order of magnitude increases in drainage area. Intermediate reaches (link midpoints along gullies) follow the same slope–drainage area trend observed in the gully heads at drainage areas less than approximately  $10^6 \text{ m}^2$  and gradients larger than  $0.35 \text{ m m}^{-1}$  or  $19^\circ$  (Fig. 10). At slopes below the  $0.35 \text{ m m}^{-1}$ , intermediate reaches become more scattered, and suggest a possible transition to a slope–drainage area relationship where large reductions in slope accompany modest increases in drainage area

(relative to the slope–area trend observed above  $0.35 \text{ m m}^{-1}$ ). Downstream limits of gullies are the most scattered of the three sets of measurements, but generally cluster with intermediate reaches below a slope of  $0.35 \text{ m m}^{-1}$  (Fig. 10). For comparison, Stock and Dietrich (2003) attributed curved plots of slope and drainage area along valleys to a change in the dominant mode of erosion from debris flows (low concavity at small drainage areas) to fluvial erosion, and observed slope–area scaling breaks at drainage areas ranging from  $10^4$  to  $10^6 \text{ m}^2$  and at slopes of  $0.10 \text{ m m}^{-1}$  ( $\sim 6^\circ$ ).

Measured infiltration capacity across the sediment covered, unvegetated locations averaged  $6.6 \pm 5.1 \text{ cm h}^{-1}$  ( $1\sigma$ ), generally exceeding the maximum hourly rainfall rates of  $\sim 2 \text{ cm h}^{-1}$  recorded during the 2006 storm.

## 5.2. Drainage networks in proglacial areas

Expanding upon the measurements of slope and drainage area along individual gullies where debris flows initiated in 2006, slope and drainage area distributions within drainage networks in proglacial areas reveal morphological differences between DFB and NDFB. Differences in slope–drainage area distributions explain well spatial patterns of debris flows in the 2006 storm. The NL and LCC metrics across the defined slope–drainage area partitions reveal differences in slope and drainage areas between DFB and NDFB. Fig. 11 shows cumulative metrics for each of the partitions defined in Fig. 7, allowing examination of the differences in slope and drainage area distributions in each basin type. On average, slopes and drainage areas similar to those of known debris flow gullies characterized a greater length of the drainage network in DFB than NDFB as shown by the separation in respective cumulative NL curves in Fig. 11A. NDFBs generally have lower slopes and larger drainage areas. The disparity in slope–drainage area distributions is shown by the divergence in the two basin groups in cumulative NL and LCC metrics along partitions of approximately 1 and greater (Fig. 11). In general, the observed differences suggest slope of proglacial areas differentiated DFB from NDFB, where high gradients were associated with debris flows.

The LCC metric explains differences between the two basin types better than the NL metric given  $t$ -tests for differences in means assuming unequal variances (compare  $p$ -values in Fig. 11A and B). For the same slope–area partitions (above values of  $\sim 1$ ) in the vicinity of slope–area trends observed among debris flow gullies, the LCC metric consistently had greater statistical significance in defining basin differences than the NL metric (Fig. 11). That LCC better differentiates basins than NL suggests gully length above slope–drainage area thresholds may also be a controlling factor in debris flow initiation within gullies.

Simple measures of glacier extent show that debris flow basins tend to have smaller glaciers, and that debris flow occurrence in the 2006 storm appears unrelated to the degree of glacier retreat from 1970 to 2008 (Sisson et al., 2011). Statistically significant differences ( $p < 0.05$ , two-tail  $t$ -test assuming unequal variances) in mean and maximum elevation and maximum drainage area characterize proglacial areas of the two basin types, indicating that proglacial areas of DFB occur at higher elevations and smaller drainage areas than those of NDFB (Table 1). Because the down-valley extent of a glacier determines where a proglacial area sits, drainage area and elevation of proglacial areas reflect glacier extent. The coincidence between high elevations and higher slopes in DFB, as reflected by the NL and LCC metrics, likely reflects positive slope–elevation trends in the elevation band of glacier termini for the volcano as a whole (Fig. 12). Differences in glacier retreat between the two basin types, however, are insignificant (Table 1).

## 6. Discussion

Debris flows in 2006 storm on Mount Rainier were initiated from proglacial gullies in seven basins. Gully heads at or near glacier termini suggest that surface runoff carrying minimal coarse sediment was

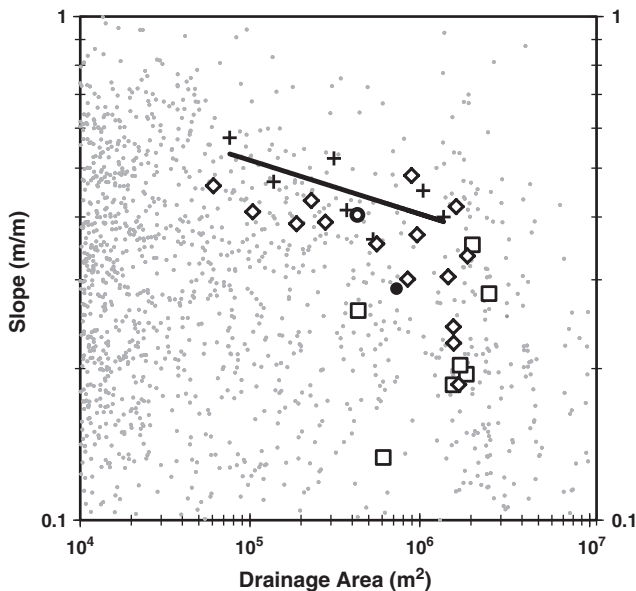


**Fig. 10.** Slope–drainage area plot of the 2006 debris flow gullies. Gully heads (crosses), intermediate reaches (diamonds), and downstream limits (squares) of the seven debris flow gullies are shown. The solid line indicates a power regression of the gully heads ( $S = 1.769A^{-0.107}$ ;  $R^2 = 0.477$ ). Small gray dots represent all extracted links of drainage networks in all proglacial areas, and are the data used in the slope–drainage area partition analysis. Large circles show the length-weighted average of slope and drainage area for the two basin types (open = DFB, filled = NDFB), which appear skewed toward large drainage areas relative to the distribution of points because links with larger drainage areas are also longer.

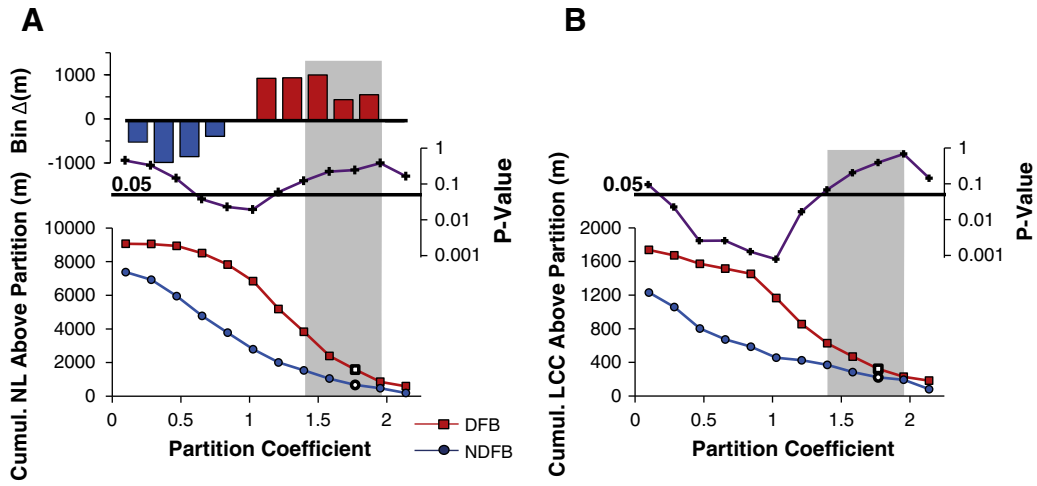


**Fig. 11.** Partition graphs for two defined metrics of network length (NL, A) and longest connected channel (LCC, B). Partition coefficients define partitions in slope–drainage area space shown in Fig. 7. Metric values represent the cumulative length of the drainage network with slope and drainage area above a given slope–area partition. *p*-Values (*t*-test for difference of means, assumed unequal variances) correspond to values shown in cumulative plots below. The *p*-value vertical axis is logarithmic to display differences between the two metrics. Gray boxes indicate the zone of slope and drainage area observed in the upper parts of debris flow gullies. Panel A includes a bar graph showing NL within bins defined by adjacent partitions where positive values show a greater length in DFB, and negative values show a greater length in NDFB.

converted to debris flow along gullies (Fig. 1). The coincidence between expanded gullies in proglacial areas and mapped debris flows in downstream areas in all DFB studied implies that gully walls provide some portion of the sediment entrained in the debris flows.

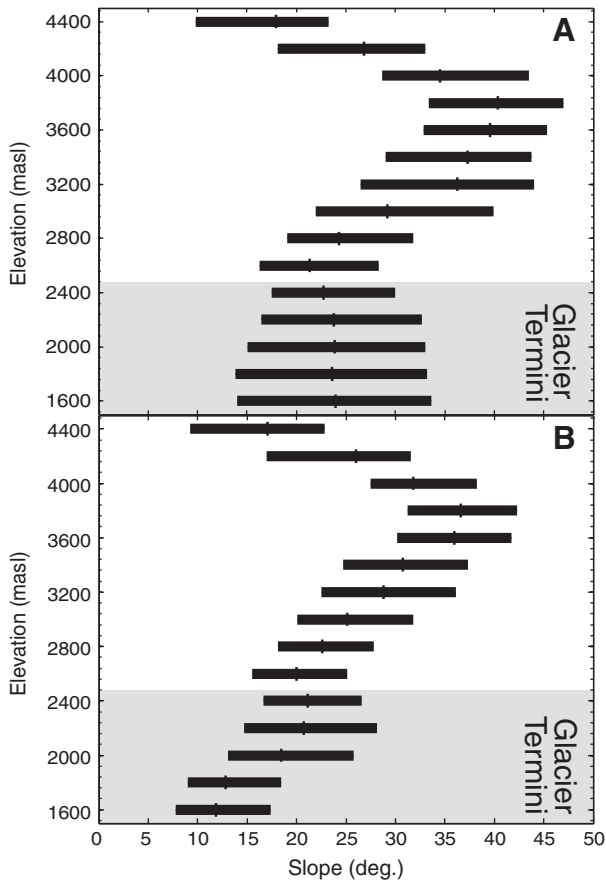


**Fig. 12.** Box plots of slope versus elevation. Slope data is binned in 200-m bands. Median slope (tick) and 25th and 75th percentile slopes (box ends) are shown for each elevation bin. (A) Slope–elevation data extracted from the DEM of the entire volcano. (B) Slope–elevation data extracted from only 1970 glacier extents, which effectively selects for valley bottoms containing existing proglacial areas.

Slope–drainage area relations at heads of gullies where debris flows were initiated suggest that failure of gully beds may play an unseen, but central role in debris flow initiation. Flume experiments and theoretical formulations reveal that debris flow initiation due to channel-bed failure begins above a threshold slope where the critical Shields stresses required for fluvial sediment transport are greater than those for debris flow transport (Lamb et al., 2008; Prancevic et al., 2014). Depending on sediment size, sorting, and shape, the threshold slope separating debris flow and fluvial transport ranges from 15° to 30°. Heads of gullies where debris flows were initiated are generally the steepest points along the gullies, and had a minimum slope of 0.35 m m<sup>-1</sup> (19°; Fig. 10). The minimum gully head slope falls within the range found by Prancevic et al. (2014). The larger set of slope–drainage area measurements along the seven debris flow gullies (gully heads, intermediate reaches, and downstream ends) reveals a scaling break at 0.35 m m<sup>-1</sup> as well. At slopes above 0.35 m m<sup>-1</sup>, slope–area measurements at intermediate reaches of debris flow gullies align with the power-law regression fit of gully heads only (Fig. 10). Below slopes of 0.35 m m<sup>-1</sup>, slope–area measurements along lower portions of gullies (intermediate reaches and downstream-most points) are scattered, suggesting a possible transition from debris flow to fluvial sediment transport and erosion with increasing drainage area (Stock and Dietrich, 2003; Prancevic et al., 2014).

The slope–drainage area trends measured here are similar in shape to those observed in longitudinal profiles of bedrock valleys, where low channel concavity is associated with bedrock erosion by debris flows and scaling breaks mark the transition to bedrock erosion by fluvial processes (Stock and Dietrich, 2003, 2006). Scaling breaks occur at slopes of approximately .10 m m<sup>-1</sup> (6°) for longitudinal profiles of bedrock channels (Stock and Dietrich, 2003). The scaling breaks in bedrock channels occur at slopes well below the minimum slope of 19° at the heads of debris flow gullies in this study. Differences between the threshold implied by the debris flow gullies and scaling breaks found by Stock and Dietrich (2003) may be a result of debris flow erosion occurring along run-out tracks as well as initiation zones in bedrock channels, and landscape differences, reflecting steady-state conditions in bedrock channels of Stock and Dietrich (2003) relative to the disequilibrium volcanic landscape of Mount Rainier.

Interestingly, a relatively minor portion of the drainage network in sediment-covered proglacial areas appears to lie above the slope–area trend observed at debris flow gully heads (see small gray dots relative to gully measurements in Fig. 10, as well as the general paucity of slope and drainage areas above partitions of 2 in Fig. 11), which may

provide insights into the evolution of steep gullies. The paucity of slope and drainage areas above the trend observed in gully heads may suggest that gullies with sediment beds reduce in gradient toward a critical threshold for debris flow initiation (Prancevic et al., 2014). This possible relaxation of gully beds is an important consideration for debris flow hazards through time. If, for instance, longitudinal (and cross-sectional) slopes of debris flow gullies were lessened as a result of debris flows in the 2006 storm, greater runoff would be required to push the same gullies beyond the critical Shields stress for debris flow transport in future storms.

Debris flow initiation was not observed or measured directly, so the primary processes involved in debris flow initiation can only be inferred. The correspondence between laterally expanded gullies and debris flow deposits downstream alone suggests gully expansion plays some integral role in debris flow initiation. However, no theory is currently available to explain debris flow initiation in gullies as a result of solely lateral expansion and sediment bulking. Slope–drainage area observations imply erosion thresholds (Montgomery and Dietrich, 1994), and may suggest failure of the bed as the primary initiation mechanism in gullies. If bed failure is the primary initiation mechanism, lateral expansion may occur in response to bed failure. In this case, gully wall failure likely contributes sediment volume to debris flows traveling down gullies. The estimated volume of material lost from gully walls alone suggests that they likely provided a significant volume of sediment to the debris flows in 2006, which would have enhanced impacts to downstream areas (Rickenmann, 1999).

A hybrid model integrates debris flow initiation by bed failure near gully heads and sediment recruitment from gully walls at increasing rates downstream, followed by subsequent transport and minor entrainment as the debris flow transits downstream to channel reaches with lower slopes. In the Pyramid gully, sediment yield from gully walls was greatest in the middle portion of the gully, where slopes are similar to the  $0.35 \text{ m m}^{-1}$  minimum observed at gully heads (sub-reach 2, Figs. 9 and 10). Increasing yield along upper gullies is a common observation along debris flow gullies in burned areas (Santi et al., 2008). Long gullies above some slope threshold for debris flow initiation with abundant unstable sediment at their margins would therefore have a greater likelihood of generating debris flows of sufficient volumes to be detected downstream. The basin comparison using the LCC metric suggests that gully length, as well as slope, distinguished debris flow and non-debris flow basins (Fig. 11), providing possible support for gully length and sediment recruitment along gullies as factors in initiation of the debris flows in the 2006 storm.

Sparse monitoring data currently limits the ability to constrain runoff generation on the upper volcanic slopes. Infiltration rates of sediment-covered upper slopes ( $\sim 6 \text{ cm h}^{-1}$ ) generally exceed the rainfall rates measured in the storm ( $\sim 2 \text{ cm h}^{-1}$ ). SNOTEL data from November 2006 reveal above-freezing temperatures, freezing altitudes near Mount Rainier's summit, and minimal snow depths during the storm (Fig. 2). Snow levels at higher elevations, however, are largely unknown. Rain-on-snow appears to be one possible mechanism for generating the runoff for debris flow initiation given that the SNOTEL station sits at the lower end of the elevation band encompassing debris

flow initiation gullies (Harr, 1981). The role of glaciers in generating runoff is also uncertain. All debris flow gullies are downstream of glaciers or permanent ice, implying that glaciers contributed an unconstrained amount of runoff. Glaciers on Mount Rainier have varying surface topography and roughness, sediment coverage, and crevasse abundance, all of which may influence rainfall infiltration into glaciers. The end-of-summer (fall) timing of the 2006 storm (common to many other debris flow-producing storms on Mount Rainier; Copeland, 2009) suggests that englacial conduits were integrated, which facilitates through-flow of rain water infiltrating glacier surfaces (Walder and Driedger, 1995; Anderson, 2004). Alternatively, glaciers may hold greater volumes of snow than surrounding sediment and bedrock surfaces, providing enhanced runoff to proglacial areas below.

The comparative analysis of proglacial areas and their drainage networks oversimplifies debris flow initiation on Mount Rainier in two ways. First, debris flows may occur in periglacial areas along the sides of glaciers, areas outside of this study's analysis window. The debris flows identified and studied here, however, apparently initiated in proglacial areas with limited input from lateral periglacial regions (Fig. 1). Secondly, our assumption that all gullies and channels in proglacial drainage networks have an unlimited supply of sediment available is not strictly correct. For instance, gullies that undercut large accumulations of glacial till have greater material volume available to be recruited, whereas other gullies adjacent to bedrock outcrops have limited access to transportable material. The effect of variable supply may explain the statistical scatter in results, but does not appear to be a major limiting factor on debris flow initiation in the 2006 storm.

The spatial distribution of debris flow-producing basins and their relationship to volcanic shape (Fig. 12) explains the relationship between glacier extent within a catchment and debris flow potential. Drainage network steepness in proglacial areas reflects the distribution of debris flows in the 2006 storm, as shown by statically significant differences in slope–drainage area distributions in Fig. 11. Elevations and maximum drainage areas demonstrate that glacier termini and proglacial areas in DFB are located higher on the volcano than NDFB (Table 1). Proglacial areas occupying higher positions on the volcano thus tend to be steeper and more favorable for debris flow initiation. The patterns of proglacial slope and elevation reflects the overall increase of slope with elevation on the Mount Rainier edifice (Fig. 12).

Observations of slope, glacier extent, and elevation reflect a simple model that links glacier extent to debris flow production (Fig. 13). Debris flow production is coupled to the slope distribution within a catchment to a first order, and in particular the slope distribution in proglacial areas where debris and water availabilities are large. Because of positive slope–elevation trends observed on the Mount Rainier edifice (Fig. 12), variable glacier extent down the flanks of the volcano in space and time control the slope of the proglacial sediment veneer. Fig. 13 conceptually shows variable glacier size across three climatic periods and how the locations of corresponding glacier termini relative to debris flow initiation thresholds may create different combinations of debris flow occurrence. Sediment supply seems not to be the greatest limiting factor on spatial patterns of debris flow generation for the debris flows studied here. If sediment supply was the limiting factor,

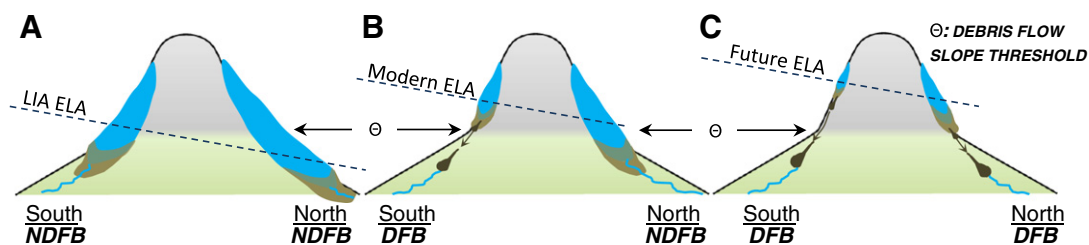


Fig. 13. Conceptual diagram of spatial and temporal variation in glacier size and its control on debris flow occurrence. Equilibrium line altitude (ELA) and corresponding glacial extent are shown for the Little Ice Age (LIA, A), present day (B), and for a future scenario when ELA is higher (C).

basins with the most glacial retreat and greatest proglacial areas ought to have the greatest debris flow potential. The aerial extent of sediment exposed by retreating glaciers appears to have had little influence on the spatial patterns of debris flow occurrence in the 2006 event. Debris flow likelihood increases in response to enhanced sediment supply (e.g. Chiarle et al., 2007) only in the event that surface slope angle is sufficiently high for debris flow initiation.

A concern for glaciated alpine areas is how debris flow hazard changes in response to a warming climate, retreating glaciers, and changing storm patterns. In a simplistic sense, retreating glaciers and changing storms potentially increase the sediment, water, and/or energy (slope) available for debris flow initiation (Moore et al., 2009; Schneuwly-Bollschweiler and Stoffel, 2012). The geology, geomorphology, and morphology of a basin dictate sensitivity to potential climate-related changes. Increases in debris flow occurrence as glaciers retreat and expose steep slopes, for example, are suggested by the 2006 event on Mt. Rainier (Fig. 13). Debris flow occurrence in a basin with a retreating glacier, however, is likely to be unchanged if slope of the proglacial region was sufficiently steep for debris flow initiation prior to retreat assuming sediment availability remains constant.

Debris flow occurrence is thought to be sensitive to changes in storm frequency and intensity where the volumes of sediment available are great (Bovis and Jakob, 1999). The abundant sediment supply from large glaciers and extensive hydrothermal alteration implies that the upper flanks of the Cascade Volcanoes have a seemingly unlimited sediment supply above and beyond the sediment produced during glacial retreat (Crowley and Zimbleman, 1997; John et al., 2008). Yet, the fact that debris flows originate from evolving gully networks hints toward a subtle complication in forecasting future probabilities. Gully development, adjustment, and relaxation accompany progressive channelization of un-dissected sediment in proglacial areas (Ireland et al., 1939; Curry et al., 2006). If that landscape adjustment is accompanied by lowering of longitudinal and side slopes of gullies, probabilities of debris flow initiation reduce substantially despite the fact that the sediment present remains high. In the European Alps, periglacial gullies where debris flows were initiated stabilized within approximately 50 years of incision (Curry et al., 2006). The seven debris flow gullies studied here pass through areas deglaciated since the end of the Little Ice Age (<150 years before present), but their stability remains in question. Thus, an important and unresolved question is what controls the development and evolution of steep gullies in deglaciated areas.

## 7. Conclusions

Debris flow initiation from high mountain peaks during intense storms is fundamentally a difficult process to observe directly, but is also an essential process to understand due to its implications for downstream areas. Analysis of debris flow gullies from one large storm in 2006 revealed the processes and conditions for debris flow initiation in proglacial gullies. Seven debris flows from seven separate catchments initiated from gullies, incised into sediments exposed no earlier, and in many cases more recently than the end of the Little Ice Age. Detailed measurements of change along a single gully as well as observations of change along six other gullies (Copeland, 2009) reveal the importance of sediment contributions from gully walls in debris flow initiation. Comparisons of proglacial drainage networks between debris flow and non-debris flow basins implied that gully length as well as slope influences debris flow potential, further supporting the importance of sediment recruitment along gullies in debris flow initiation.

Slope measurements at gully heads exceed  $19^\circ$  ( $0.35 \text{ m m}^{-1}$ ) and fall within the range of slope thresholds predicted for in-channel debris flow initiation due to bed failure (Prancevic et al., 2014). Lower portions of debris flow gullies reveal a possible break in graphical slope between slope and drainage area at the same slope of  $19^\circ$ , suggesting a possible transition from debris flow to fluvial sediment transport and erosion with increasing drainage area (*sensu* Stock and Dietrich, 2003). If bed

failure, suggested by slope–area relationships, is the initiation mechanism for these debris flows, then the observed lateral expansion of gullies may be a consequence of bed failure. Gully walls therefore act as a source for sediment recruitment by debris flows. A hybrid model of debris flow initiation in gullies therefore includes bed failure near gully heads followed by sediment recruitment and debris flow volume increases along gully lengths.

The interactions and interrelationships between glaciers, glacier change, and sediment routing by debris flows and floods define a large component of a basin's geomorphic response to climatic change in many alpine environments. This study elucidates these interrelationships in a landscape highly sensitive to climate change, owing to a landscape with large maritime glaciers (Meier, 1984), an abundance of unsolicited sediment, and easily eroded bedrock. A comparison of debris flow and non-debris flow-producing basins reveals slope as the major control on spatial patterns of debris flows in the 2006 storm. Because of positive slope–elevation trends, glacier extent controls the surface gradients on sediment-covered surfaces immediately in front of glaciers. Large glaciers terminate on the lower elevation, low slopes of the volcano, whereas steep proglacial and deglaciated areas characterize the termini of relatively small glaciers that terminate at higher elevations. Therefore, glacier change has corresponding changes in the available slopes for debris flow initiation that should be considered when evaluating hazards under a warming climate.

## Acknowledgments

The National Park Service (Mount Rainier National Park) provided generous funding and field support (NPS Interagency Agreement P13PG00049). This study was also supported by graduate student research grants from the Geological Society of America (9586-11) and Mazamas Organization, a fellowship provided by George Sharp (OSU-CEOAS department fellowship), a National Center for Airborne Laser Mapping (NCALM) seed grant (WA12\_Legg), and a grant from the National Science Foundation's Geomorphology and Land Use Dynamics Program (EAR-0844017). The authors thank Trevor Waldien, K. Sean Daniels, and Anna Stifter for field assistance. Discussion with Scott Anderson, Stephen Lancaster, Chris Magirl, Anne Nolin, and Michael Olsen helped develop the ideas in this paper. Suggestions from three anonymous reviewers and Richard Whittecar were greatly appreciated and improved this manuscript substantially.

## References

- Anderson, R.S., 2004. Strong feedbacks between hydrology and sliding of a small alpine glacier. *J. Geophys. Res.* 109, F03005. <http://dx.doi.org/10.1029/2004JF000120>.
- Benda, L.E., Cundy, T.W., 1990. Predicting deposition of debris flows in mountain channels. *Can. Geotech. J./Rev. Can. Geotech.* 27, 409–417.
- Bovis, M.J., Jakob, M., 1999. The role of debris supply conditions in predicting debris flow activity. *Earth Surf. Process. Landf.* 24, 1039–1054.
- Burbank, D.W., 1981. A chronology of late Holocene glacier fluctuations on Mount Rainier, Washington. *Arct. Alp. Res.* 13, 369–386.
- Cannon, S.H., Reneau, S.L., 2000. Conditions for generation of fire-related debris flows, Capulin Canyon, New Mexico. *Earth Surf. Process. Landf.* 25, 1103–1121.
- Chiarle, M., Iannotti, S., Mortara, G., Deline, P., 2007. Recent debris flow occurrences associated with glaciers in the Alps. *Glob. Planet. Chang.* 56, 123–136.
- Coe, J.A., Kinner, D.A., Godt, J.W., 2008. Initiation conditions for debris flows generated by runoff at Chalk Cliffs, central Colorado. *Geomorphology* 96, 270–297.
- Copeland, E.A., 2009. Recent Periglacial Debris Flows from Mount Rainier, Washington (Master's). Oregon State University, Corvallis.
- Costa, J.E., 1988. Rheologic, geomorphic, and sedimentologic differentiation of water floods, hyperconcentrated flows, and debris flows. In: Baker, V.R., Kochel, R.C., Patton, P.C. (Eds.), *Flood Geomorphology*. John Wiley and Sons, New York, pp. 113–122.
- Crandell, D.R., 1971. Postglacial lahars from Mount Rainier volcano, Washington. USGS Prof. Pap. 677, 75.
- Crowley, J.K., Zimbleman, D.R., 1997. Mapping hydrothermally altered rocks on Mount Rainier, Washington, with airborne visible/infrared imaging spectrometer (AVIRIS) data. *Geology* 25, 559.
- Curry, A.M., Cleasby, V., Zukowskyj, P., 2006. Paraglacial response of steep, sediment-mantled slopes to post-“Little Ice Age” glacier recession in the central Swiss Alps. *J. Quat. Sci.* 21, 211–225.
- Czuba, J., Czuba, C.R., Magirl, Christopher S., Voss, F.D., 2010. Channel-conveyance capacity, channel change, and sediment transport in the lower Puyallup, White, and Carbon

- Rivers, western Washington. Special Investigations Report No. 5240. US Geological Survey.
- Czuba, J.A., Magirl, Christopher S., Czuba, C.R., Grossman, E.E., Curran, C.A., Gendaszek, A.S., Dinicola, R.S., 2011. Sediment load from major rivers into Puget Sound and its adjacent waters. Fact Sheet US Geological Survey, Washington Water Science Center.
- Czuba, J.A., Olsen, T.D., Czuba, C.R., Magirl, Christopher S., Gish, C.C., 2012. Changes in Sediment Volume in Alder Lake, Nisqually River Basin, Washington, 1945–2011 (No. OFR-2012-1068). United States Geological Survey.
- Dietrich, W.E., Dunne, T., 1978. Sediment budget for a small catchment in mountainous terrain. *Z. Geomorphol. Suppl.* 29, 191–206.
- Driedger, C.L., Kennard, P.M., 1984. Ice Volumes on Cascade Volcanoes: Mount Rainier, Mount Hood, Three Sisters, and Mount Shasta. US Dept. of the Interior, Geological Survey.
- Gabet, E.J., Bookter, A., 2008. A morphometric analysis of gullies scoured by post-fire progressively bulked debris flows in southwest Montana, USA. *Geomorphology* 96, 298–309.
- Gabet, E.J., Sternberg, P., 2008. The effects of vegetative ash on infiltration capacity, sediment transport, and the generation of progressively bulked debris flows. *Geomorphology* 101, 666–673.
- Hack, J.T., 1973. Stream-profile analysis and stream-gradient index. *J. Res. U.S. Geol. Surv.* 1, 421–429.
- Hack, J.T., Goodlett, J.C., 1960. Geomorphology and forest ecology of a mountain region in the central Appalachians. USGS Prof. Pap. 347, 66.
- Harr, R.D., 1981. Some characteristics and consequences of snowmelt during rainfall in western Oregon. *J. Hydrol.* 53, 277–304.
- Heliker, C., Johnson, A., Hodge, S., 1984. Nisqually glacier, Mount Rainier, Washington, 1857–1979: a summary of the long-term observations and a comprehensive bibliography. USGS Open-file Report 83-541 1984 (20 pp., 4 Figs., 5 Tabs., 84 Refs.).
- Hildreth, W., 2007. Quaternary magmatism in the Cascades—geologic perspectives. *U.S. Geol. Surv. Prof. Pap.* 1744, 125.
- Hunger, O., Morgan, G.C., Kellerhals, R., 1984. Quantitative analysis of debris torrent hazards for design of remedial measures. *Can. Geotech. J.* 21, 663–677.
- Ireland, H.A., Sharpe, C.F.S., Eargle, D., 1939. Principles of Gully Erosion in the Piedmont of South Carolina. US Dept. of Agriculture.
- Iverson, R.M., 1997. The physics of debris flows. *Rev. Geophys.* 35, 245–296.
- Iverson, R.M., Reid, M.E., LaHusen, R.G., 1997. Debris flow mobilization from landslides. *Annu. Rev. Earth Planet. Sci.* 25, 85–138.
- James, L.A., Watson, D.G., Hansen, W.F., 2007. Using LiDAR data to map gullies and head-water streams under forest canopy: South Carolina, USA. *Catena* 71, 132–144.
- John, D.A., Sisson, T.W., Breit, G.N., Rye, R.O., Vallance, J.W., 2008. Characteristics, extent and origin of hydrothermal alteration at Mount Rainier Volcano, Cascades Arc, USA: implications for debris-flow hazards and mineral deposits. *J. Volcanol. Geotherm. Res.* 175, 289–314.
- Kean, J.W., Staley, D.M., Cannon, Susan H., 2011. In situ measurements of post-fire debris flows in southern California: comparisons of the timing and magnitude of 24 debris-flow events with rainfall and soil moisture conditions. *J. Geophys. Res.* 116, F04019. <http://dx.doi.org/10.1029/2011JF002005>.
- Kean, J.W., McCoy, S.W., Tucker, Gregory E., Staley, D.M., Coe, Jeffrey A., 2013. Runoff-generated debris flows: observations and modeling of surge initiation, magnitude, and frequency. *J. Geophys. Res. Earth Surf.* 118, 2190–2207.
- Lamb, M.P., Dietrich, W.E., Venditti, J.G., 2008. Is the critical Shields stress for incipient sediment motion dependent on channel-bed slope? *J. Geophys. Res. Earth Surf.* 113, F02008. <http://dx.doi.org/10.1029/2007JF000831>.
- Lancaster, S.T., Nolin, A.W., Copeland, E.A., Grant, G.E., 2012. Periglacial debris-flow initiation and susceptibility and glacier recession from imagery, airborne LiDAR, and ground-based mapping. *Geosphere* 8, 417–430.
- Meier, M.F., 1984. Contribution of small glaciers to global sea level. *Science* 226, 1418–1421.
- Meyer, G.A., Wells, S.G., 1997. Fire-related sedimentation events on alluvial fans, Yellowstone National Park, USA. *J. Sediment. Res.* 67, 776–791.
- Meyer, G.A., Wells, S.G., Jull, A.J.T., 1995. Fire and alluvial chronology in Yellowstone National Park: climatic and intrinsic controls on Holocene geomorphic processes. *Geol. Soc. Am. Bull.* 107, 1211–1230.
- Mills, H.H., 1976. Estimated erosion rates on Mount Rainier, Washington. *Geology* 4, 401–406.
- Montgomery, D.R., Dietrich, W.E., 1994. Landscape dissection and drainage area–slope thresholds. In: Kirkby, M.J. (Ed.), *Process Models and Theoretical Geomorphology*. John Wiley, Chichester, pp. 221–246.
- Moore, R.D., Fleming, S.W., Menounos, B., Wheate, R., Fountain, A., Stahl, K., Holm, K., Jakob, M., 2009. Glacier change in western North America: influences on hydrology, geomorphic hazards and water quality. *Hydrol. Process.* 23, 42–61.
- National Park Service, 2014. Webpage <http://www.nps.gov/mora/parknews/november-2006-flood-old-page.htm> (Accessed June 12, 2014).
- Neiman, P.J., Ralph, F.M., Wick, G.A., Kuo, Y.H., Wee, T.K., Ma, Z., Taylor, G.H., Dettinger, M.D., 2008. Diagnosis of an intense atmospheric river impacting the Pacific Northwest: storm summary and offshore vertical structure observed with COSMIC satellite retrievals. *Mon. Weather Rev.* 136, 4398–4420.
- O'Connor, J.E., Hardison, J.H., Costa, J.E., 2001. Debris flows from failures of Neoglacial-Age moraine dams in the Three Sisters and Mount Jefferson wilderness areas, Oregon. USGS Prof. Pap. 1606, 93.
- Pierson, T.C., 2005. Distinguishing between debris flows and floods from field evidence in small watersheds. USGS Fact Sheet, 2004-3142.
- Porter, S.C., 1989. Some geological implications of average Quaternary glacial conditions. *Quat. Res.* 32, 245–261.
- Prancevic, J.P., Lamb, M.P., Fuller, B.M., 2014. Incipient sediment motion across the river to debris-flow transition. *Geology* 42, 191–194.
- Rickenmann, D., 1999. Empirical relationships for debris flows. *Nat. Hazards* 19, 47–77.
- Santi, P.M., deWolfe, V.G., Higgins, J.D., Cannon, S.H., Gartner, J.E., 2008. Sources of debris flow material in burned areas. *Geomorphology* 96, 310–321.
- Schneuwly-Bollschweiler, M., Stoffel, M., 2012. Hydrometeorological triggers of periglacial debris flows in the Zermatt valley (Switzerland) since 1864. *J. Geophys. Res.* 117, F02033. <http://dx.doi.org/10.1029/2011JF002262>.
- Scott, K.M., Vallance, J.W., Pringle, P.T., 1995. Sedimentology, behavior, and hazards of debris flows at Mount Rainier, Washington. USGS Prof. Pap. 1547, 56.
- Sigafoos, R.S., Hendricks, E.L., 1972. Recent activity of glaciers of Mount Rainier, Washington. USGS Prof. Pap. 387-B, 24.
- Sisson, T.W., Robinson, J.E., Swinney, D.D., 2011. Whole-edifice ice volume change A.D. 1970 to 2007/2008 at Mount Rainier, Washington, based on LiDAR surveying. *Geology* 39, 639–642.
- Stock, J., Dietrich, W.E., 2003. Valley incision by debris flows: evidence of a topographic signature. *Water Resour. Res.* 39 (4), 1089. <http://dx.doi.org/10.1029/2001WR001057>.
- Stock, J.D., Dietrich, W.E., 2006. Erosion of steepland valleys by debris flows. *Geol. Soc. Am. Bull.* 118, 1125–1148.
- Tarboton, D.G., Bras, R.L., Rodriguez-Iturbe, I., 2006. On the extraction of channel networks from digital elevation data. *Hydrol. Process.* 5, 81–100.
- Vallance, J.W., Scott, K.M., 1997. The Osceola mudflow from Mount Rainier: sedimentology and hazard implications of a huge clay-rich debris flow. *Geol. Soc. Am. Bull.* 109, 143–163.
- Walder, J.S., Driedger, C.L., 1994a. Rapid geomorphic change caused by glacial outburst floods and debris flows along Tahoma Creek, Mount Rainier, Washington, USA. *Arct. Alp. Res.* 26, 319–327.
- Walder, J.S., Driedger, C.L., 1994b. Geomorphic change caused by outburst floods and debris flows at Mount Rainier, Washington with emphasis on Tahoma Creek Valley. US Geological Survey Water-Resources Investigations Report 93-4093.
- Walder, J.S., Driedger, C.L., 1995. Frequent outburst floods from South Tahoma Glacier, Mount Rainier, USA: relation to debris flows, meteorological origin and implications for subglacial hydrology. *J. Glaciol.* 41, 1–10.
- Wells, W.G., 1987. The effects of fire on the generation of debris flows in southern California. *Rev. Eng. Geol.* 7, 105–114.
- Whipple, K.X., Tucker, G.E., 1999. Dynamics of the stream-power river incision model: implications for height limits of mountain ranges, landscape response timescales, and research needs. *J. Geophys. Res.* 104, 17661–17674.
- Yang, C.T., 1972. Unit stream power and sediment transport. *J. Hydraul. Div.* 98, 1805–1826.